CARBON 66 (2014) 619–628

Available at www.sciencedirect.com

ScienceDirect

journal homepage: www.elsevier.com/locate/carbon

Orientation dependence of the fracture behavior of graphene

Young I. Jhon [a,b,*], Young Min Jhon [c], Geun Y. Yeom [b], Myung S. Jhon [a,d,*]

[a] SKKU Nano-convergence Core Technology for Human Interface (WCU), Suwon 440-746, Republic of Korea
[b] School of Advanced Materials Science and Engineering, Sungkyunkwan University, Suwon 440-746, Korea
[c] Sensor System Research Center, Korea Institute of Science and Technology, Seoul 136-791, Korea
[d] Department of Chemical Engineering, Carnegie Mellon University, Pittsburgh, PA 15213, USA

ARTICLE INFO

Article history:
Received 9 July 2013
Accepted 21 September 2013
Available online 30 September 2013

ABSTRACT

Graphene has unique mechanical properties in that it is simultaneously very strong and stretchy, which severely hampers the prediction of its orientation-dependent fracture behavior based on conventional theories used for common brittle or ductile materials. For the first time, by exploring the entire range of available tensile orientations, this study reveals the unique anisotropic fracture response of graphene using molecular dynamics simulations. We found that, as the uniaxial tensile direction rotates from armchair (0°) to zigzag orientation (30°), both the tensile strength and strain remain almost constant up to an orientation angle of ~12°, then they rapidly increase (exponential growth), resulting in a remarkable degradation of the tensile strength compared to brittle fracture counterpart (inverse-sinusoidal growth). This typical fracture pattern holds for 100–700 K. We propose a model that can explain its physical origin in good agreement with the simulation results. We also found that the elastic behavior of graphene is quasi-isotropic for all tensile orientations, in contrast to its anisotropic fracture behavior. Using indentation simulations of graphene, we showed that the anisotropic/isotropic features of fracture/elasticity are also well-preserved in the two-dimensional tensile systems but its fracture anisotropicity is greatly attenuated due to the inherent sixfold symmetry of graphene.

1. Introduction

Graphene, a single layer of carbon atoms arranged in a honeycomb structure, has attracted great attention after its experimental discovery, owing to its many exceptional properties such as ultrahigh electronic mobility, superior thermal conductivity, and excellent mechanical strength [1–7]. It is thinner and stronger than any other material ever discovered. Naturally, such superlative properties of graphene have triggered its active application to a wide range of engineering fields. For instance, there have been numerous studies to improve the mechanical strengths [8–10], thermal properties [11–13], and energy conversion efficiencies [14–16] of materials by incorporating graphene into them. One of the most featured applications is the use of graphene as a supporting film for a liquid cell in transmission electron microscopy (TEM) studies [17]. In this application, the graphene membranes stay structurally intact while encapsulating the liquid tightly and allowing very feasible electron transmission for high-resolution probing of the reaction occurring in the inside liquid, which basically benefited from the high tensile strength, flexibility, and ultrathin nature of graphene. With the growing demand for such graphene-based devices and composite materials, it becomes increasingly important to understand the mechanical characteristics of graphene at a greater level of depth.

* *Corresponding authors:* Fax: +1 412 268 7139.
E-mail addresses: yijhon@kaist.ac.kr (Y.I. Jhon), mj3a@andrew.cmu.edu (M.S. Jhon).
0008-6223/$ - see front matter
http://dx.doi.org/10.1016/j.carbon.2013.09.051

A number of studies have been performed to explore the mechanical fracture phenomena of ceramics and metals, and their mechanisms are well explained by Griffith's brittle fracture theory [18,19] and the ductile fracture models for soft metals [20,21], respectively. However, graphene is neither brittle nor ductile and essentially differs from either quality. Graphene is both very strong and very stretchy, and owing to these peculiar characteristics, the orientation-dependent fracture behavior of graphene cannot be dictated by any single mechanism proposed earlier.

Great efforts have been made in characterizing the mechanical properties of graphene [5,22], including those of its defective [23–25] structures as well, where various structural defects such as Stone Wales Thrower defects [26,27] and grain boundaries [28] were examined. By nanoindentation using atomic force microscopy, Lee et al. measured Young's modulus and the intrinsic breaking strength to be 1.0 7 ± 0.1 TPa and 130 ± 10 GPa, respectively, assuming the thickness of graphene to be 0.335 nm [5]. Meanwhile, most of preceding studies on the mechanical properties of graphene have predominantly relied on computational methods such as ab initio calculations [29–31], tight-binding models [32,33], and molecular dynamics simulations [34–36] due to the tremendous experimental difficulties in controlling a monoatomic film and developing appropriate measurement techniques. From these theoretical approaches, we have been able to understand many principal characteristics of graphene, such as Poisson's ratio, the temperature effect, and the grain boundaries effect which had been extremely elusive to determine using experimental methods.

In particular, theoretical studies suggested that graphene would exhibit distinct anisotropic fracture behavior in tensile deformation, which has not yet been experimentally observed. For instance, a molecular dynamics study indicated that the tensile strength and strain of graphene are 107 GPa and 0.20 under zigzag-directional elongation while they are 90 GPa and 0.13 under armchair-directional elongation at 300 K [22]. However, all preceding studies on the tensile mechanics of graphene have been devoted merely to the zigzag and armchair directional deformations, and the tensile mechanics of other orientations have never been inspected, although graphene would be likely to deform along various directions in realistic cases.

To address this problem, in the present paper, the tensile fracture and elastic behaviors of graphene were systematically investigated using molecular dynamics simulations as the uniaxial tensile direction rotated very gradually from the armchair to the zigzag direction in the honeycomb crystal lattice of graphene. This rotational range covers the complete range of tensile orientations of graphene due to its sixfold symmetry. Specifically, nine tensile orientations were selected for this study as shown in Fig. 1a, and our uniaxial tensile simulation system is briefly illustrated in Fig. 1b.

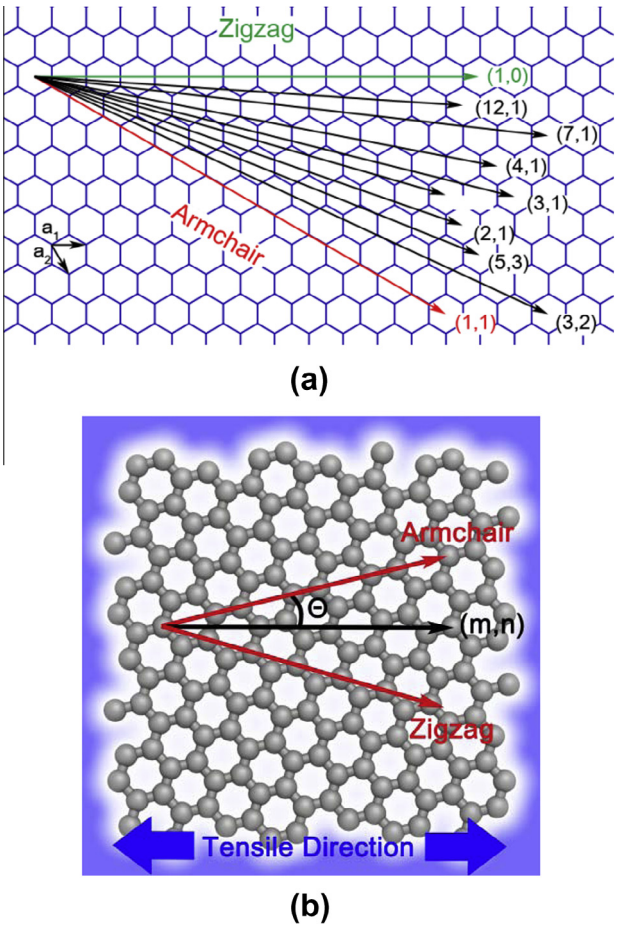

Fig. 1 – (a) The nine tensile orientations selected to investigate the orientation-dependent tensile mechanics of graphene, where the corresponding chiral notations are given in parentheses. (b) The illustrated uniaxial tensile simulation system where the tensile direction has been set to an arbitrary (*m*,*n*) chiral direction, and an orientation angle θ is defined as the angle made between the relevant tensile direction and the armchair direction. (A color version of this figure can be viewed online.)

2. Computational methods

All calculations were performed using the LAMMPS (large-scale atomic/molecular massively parallel simulator) software package [37] and the simulation systems were constructed to meet a periodic boundary condition. For interactions between carbon atoms, we employed (AIREBO) adaptive intermolecular reactive empirical bond order potential [38] which has been widely used to study the mechanical properties of carbon materials, such as carbon nanotube (CNT) [39], fullerenes [40], and graphene [24,35,41]. The cutoff radius of the potential was set to be 2.0 Å to avoid spuriously high bond forces and unphysical results near the fracture region [24,35,41]. The dimensions of the simulation system and atomic coordinates were first optimized using a gradient-based minimization method with tolerance criteria of 10^{-8} eV/Å in force and/or 10^{-8} eV in energy. Using the system size obtained above, a canonical ensemble simulation was subsequently performed for 3×10^5 steps by increasing the temperature gradually from zero to the desired temperature and further equilibrated for 7×10^5 steps under isothermal conditions. After equilibrium was reached, the system was finally elongated with a strain rate of 0.1 ns^{-1} in the

specific tensile direction where a non-equilibrium molecular dynamics simulation was employed to describe the non-thermal streaming velocities of the continuously strained system using the SLLOD equations of motion coupled to a Nose–Hoover thermostat [42].

3. Results and discussion

3.1. Orientation dependence of tensile fractures

The tensile strength of graphene is plotted as a function of an orientation angle θ, where θ is defined to be the angle made between the armchair direction and the tensile direction (Fig. 1b). For the armchair and zigzag tensile directions, θ is 0° and 30°, respectively, and θ would range between these values for an arbitrary tensile direction due to the sixfold symmetry of graphene. Noticeably, as the orientation angle increases, we found that the tensile strength remains almost constant up to an orientation angle of ~12°, then it rapidly increases (exponential growth) (Fig. 2a). This unique fracture pattern was consistently observed for all operating temperatures examined here (namely, 100, 300, 500, and 700 K), although the tensile strength quantitatively decreases as the temperature increases due to the thermal softening (Fig. 3). For the tensile fracture strain, we observed very similar orientation dependence as that of the tensile strength (Figs. 2b and S1). To see their orientation dependence more manifestly excluding the thermal effect, we also plotted the tensile strength and strain in a reduced form by dividing them with their values for an orientation angle of 0° (*i.e.*, those of the armchair tensile direction) at the various temperatures. The curves showed excellent coincidence with each other when they were put together (Fig. 2c and d), which indicates that an identical physical origin may exist behind them, regardless of the temperature.

3.2. Simplified fracture model

To gain insight into the physics of the aforementioned phenomena, we carefully monitored the structural evolution of graphene during the tensile process. We found that the fracture of graphene dominantly occurs along the zigzag-lines of the hexagonal structure, regardless of the tensile orientation and temperature (Fig. 4). Similar results were observed in the axial elongation of CNT with various chiralities as well as in the longitudinal elongation of graphene nanoribbons with armchair and zigzag edges [22,43]. In these studies, they employed a Cauchy–Born equation for homogenous deformation to predict the values of fracture strain for various tensile orientations. However, lattices with a basis like that of graphene lacks inversion symmetry and thus, graphene nanoribbons and CNT are not supposed to follow the Cauchy–Born rule precisely, as demonstrated in Dumitrica et al.'s work [43]. More importantly, the orientation-dependent tensile strengths of CNT and graphene nanoribbons have not been theoretically addressed in these studies, although the tensile strength is as or more important than the fracture strain in the characterization of graphene.

We speculated that the failure of graphene that occurs along the zigzag-lines much resembles the slip or breaking of metal crystals which takes place on the densest lattice plane under tensile deformation. Based on this idea, stress transformation formalism [44] was adopted to evaluate the tensile strength of graphene for an arbitrary tensile direction as given by:

$$S_n = \frac{1}{2}(S_x + S_y) + \frac{1}{2}(S_x - S_y)\cos 2\theta + T_{xy}\sin 2\theta \quad (1)$$

where S_n is the (engineering) stress normal to an arbitrary plane (*P*-plane) that is perpendicular to the *xy*-plane, θ is the angle made between the x-direction and the normal direction of the *P*-plane, and S_x, S_y, and T_{xy} refer to the corresponding components of the Cauchy stress tensor. We made three assumptions in this equation for the application to the uniaxial tensile fracture of graphene. First, the *x*-direction and normal direction correspond to the tensile direction and the armchair-direction that is closest to the tensile direction, respectively. Second, the values of S_y and T_{xy} are negligible during the tensile process. Third, the elongation is completed to the fracture point. The equation would then be written as:

$$S_f^{AC} = \frac{S_f^{tensile}}{\cos^2\theta_f'} \quad (2)$$

where S_f^{AC} is the tensile strength in the armchair direction, $S_f^{tensile}$ is the tensile strength in an arbitrary tensile direction, and θ_f' is the angle made between the armchair direction and the tensile direction at the tensile fracture. If we assume the brittle fracture of graphene, θ_f' should approximate to θ_0 as denoted in Fig. 5, since the initial armchair direction and the armchair direction at the tensile fracture point would be almost the same. However, graphene is not brittle and it will stretch considerably until the fracture occurs (Supplementary Movie 1). Taking this factor and a possible distortion effect into account, we roughly assumed that θ_f' of Eq. (2) should be the intersection angle measured at the tensile failure point rather than that of the original structure (Fig. 5). Considering the geometric relationship formed during the tensile process (Fig. 5), we derived the equations for several significant strains in order to eventually evaluate the magnitude of θ_f', as shown below:

$$e_{tensile} + 1 = \frac{L'}{L} = \frac{\tan\theta_0}{\tan\theta'} = \frac{\tan\theta''}{\tan\theta_0} \quad (3)$$

$$e_{AC} + 1 = \frac{L_{AC}}{L_{AC}'} = \frac{\sin\theta_0}{\sin\theta'} \quad (4)$$

$$e_{ZZ} + 1 = \frac{L_{ZZ}'}{L_{ZZ}} = \frac{\cos\theta_0}{\cos\theta''} \quad (5)$$

where $e_{tensile}$, e_{AC}, and e_{ZZ} are the tensile (engineering) strains along the tensile direction, armchair-direction, and zigzag-direction, respectively. The meanings of the other variables are depicted in Fig. 5. Providing that the magnitudes of the tensile strength $\left(S_f^{AC}\right)$ and fracture strain $\left(e_f^{AC}\right)$ of graphene are known for the armchair-directional elongation, we can evaluate the values of θ_f' and the fracture strain $\left(e_f^{tensile}\right)$ of an arbitrary tensile direction using Eqs. (3)–(5). We are also able to know the value of the tensile strength $\left(S_f^{tensile}\right)$ of an arbitrary tensile direction from the value of θ_f' using Eq. (2). Here,

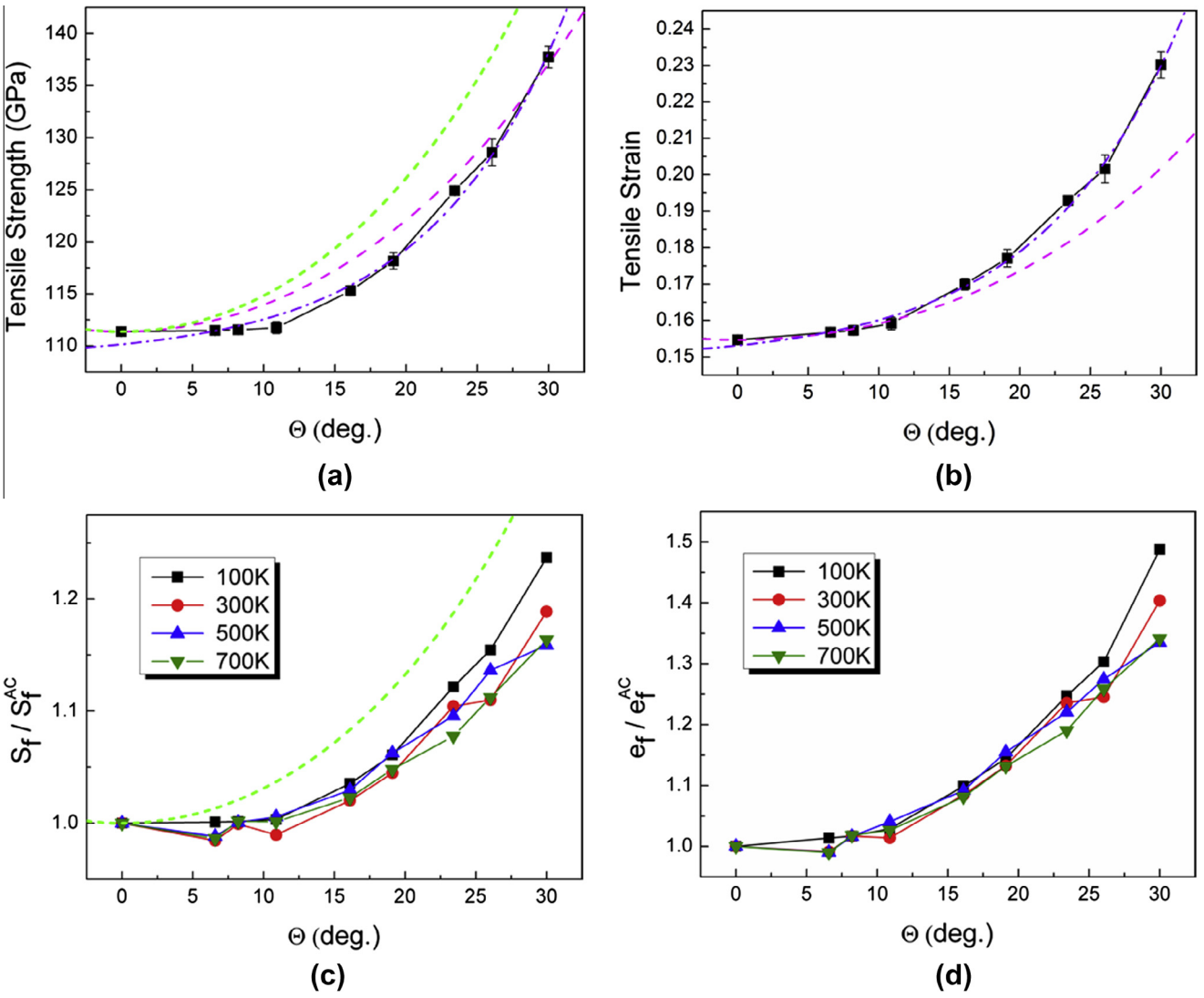

Fig. 2 – (a) The tensile strength and (b) the fracture strain of graphene plotted as a function of the orientation angle at 100 K. (c) The tensile strengths and (d) fracture strains of graphene plotted as a function of the orientation angle at various temperatures, where they are given in a reduced form such that they are divided by their respective values at the orientation angle of 0° (armchair direction) for each temperature. In (a)–(c), the magenta dashed lines and violet dot-dashed lines indicate the values obtained from our fracture model and numerical platform, respectively, while the green short-dashed line indicates the tensile strengths obtained from the brittle fracture model. (A color version of this figure can be viewed online.)

we neglected a contraction perpendicular to the tensile direction during the tensile process as is the case in most of bulk system tensile simulations.

The tensile strength and strain values predicted from this fracture model are shown by the magenta dashed lines in Figs. 2 and 3, and S1. They generally showed good agreement with the simulation results. However, the predicted values for the tensile strength somewhat deviated as the temperature increased, while the predicted values of the fracture strain showed excellent agreement regardless of the temperature. It suggests that the structural relation (to obtain fracture strain) shown in Fig. 5 is reasonable regardless of the temperature but the prediction using Eq. (2) (to obtain fracture strength) is quantitatively inaccurate at the higher temperatures presumably due to poor evaluation of the distortion effect on the tensile strength.

In contrast to this fracture model, the use of a brittle fracture model significantly overestimated the tensile strengths and its extent increased as the orientation angle increased, as shown by the green short-dashed lines in Fig. 2a and c. A maximum discrepancy of ~11.412 GPa was observed under the zigzag-directional elongation.

3.3. *Integrated numerical platform*

In order to precisely predict the fracture behavior of graphene for a whole range of tensile orientations and a wide range of operating temperatures, we constructed an integrated numerical platform that can reproduce the simulation results obtained for various orientation angles and operating temperatures. To achieve the best approximation to the sim-

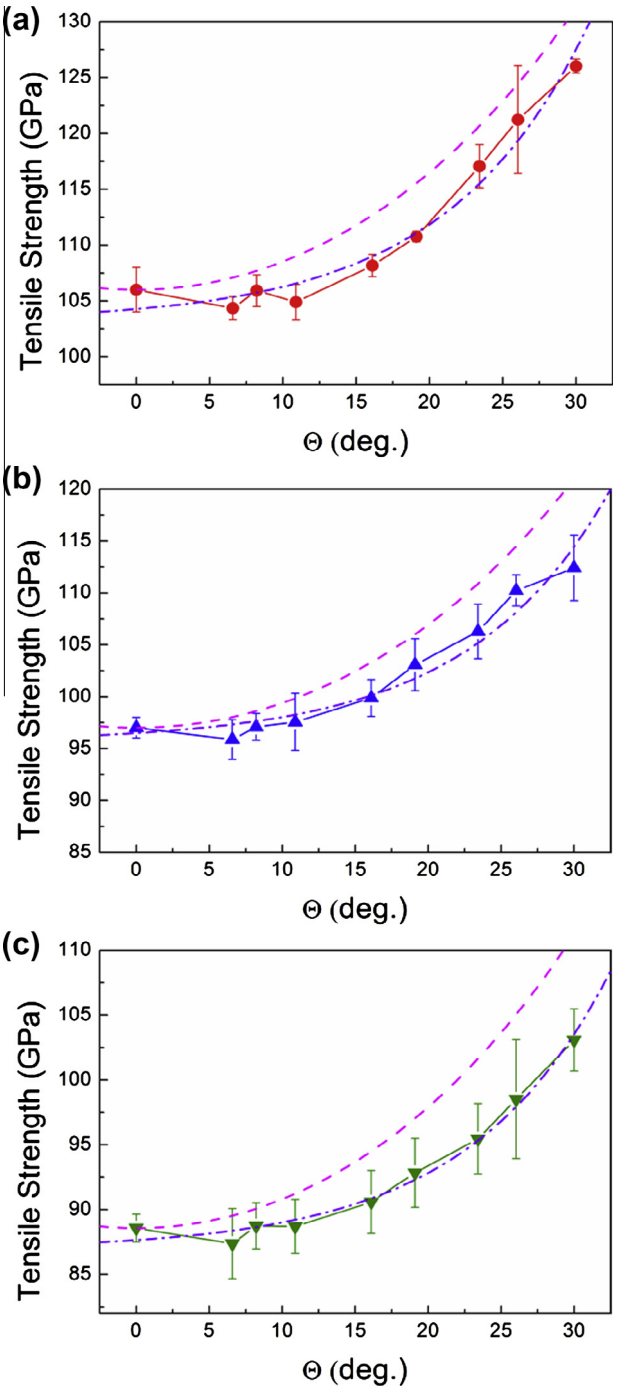

Fig. 3 – The tensile strength of graphene plotted as a function of the orientation angle at (a) 300, (b) 500, and (c) 700 K. Magenta dashed lines and violet dot-dashed lines indicate the values obtained from our fracture model and numerical platform, respectively. (A color version of this figure can be viewed online.)

ulation results, we employed an exponential growth fitting template as given by:

$$y(x) = A_0 \times \exp\left(\frac{x}{x_0}\right) + y_0 \quad (6)$$

where x is the tensile orientation angle and y is the corresponding tensile strength or fracture strain, while A_0, x_0, and y_0 are parameters to be determined by a fitting process. Based on this regime, we obtained curves which were very well fitted to the simulation results at an operating temperature of 100 K, as shown by the violet dot-dashed lines in Fig. 2a and b. We also obtained curves fitted to the simulation data of 300, 500, and 700 K in a similar manner, while maintaining the value of x_0 with that used for fitting to 100 K data, which all showed excellent agreement with the simulation results (Figs. 3 and S1). To cover all other operating temperatures located between 100 and 700 K (interpolation), possibly including the temperatures out of this range as well (extrapolation), quadratic polynomial equations of temperature were further fitted to A_0 and y_0 with very high precision (Fig. S2). The optimal parameter values obtained in this study are summarized in Tables S1 and S2. We expect that the numerical platform presented here will provide an informative mechanical guideline in various engineering fields of graphene.

3.4. *Quasi-isotropic elastic behavior*

Besides the study on orientation-dependent tensile fracture mechanics, we have also investigated how the elastic behavior of graphene changes according to variations in the tensile direction. Interestingly, the calculations indicated that graphene should exhibit quasi-isotropic elastic behavior for all tensile orientations, in contrast to its anisotropic tensile fracture behavior. In other words, almost the same magnitudes of elastic stress are required under the same strain for all different tensile orientations as far as the elongation continues prior to fracture (Fig. 6). In the previous study [22], a similar isotropic elastic response of graphene was observed for the armchair and zigzag tensile elongations. Despite this observation, however, we were not able to confirm that the elastic response of graphene is indeed (quasi) isotropic because it has never been examined for other tensile directions. In this context, our study provides the first proof of principle for this issue, and this isotropic elastic feature holds for all temperatures examined here (Fig. S3).

In Lee et al.'s indentation study [5], an isotropic mechanical response of graphene was assumed based on its sixfold rotation symmetry in deriving the equation which relates the tensile strength magnitudes and the measured values of the indenter force. Regarding this point, our finding suggests that the isotropic mechanical response of graphene would occur at a more fundamental level, as far as it is concerned to the elastic deformation.

3.5. *Two-dimensional tensile system (indentation)*

Should the anisotropic/isotropic features of the fracture/elasticity of graphene observed in the uniaxial tensile systems be preserved in two-dimensional (2D) tensile systems as well? Even if they are, is there any difference between the performances of 1D and 2D tensile systems? To address these questions, we carried out a series of molecular dynamics simulations for the indentation of graphene membranes attached on SiO_2 substrates (Fig. 7a). Details of our scheme are similar to those of Lee et al.'s experimental study[5] except

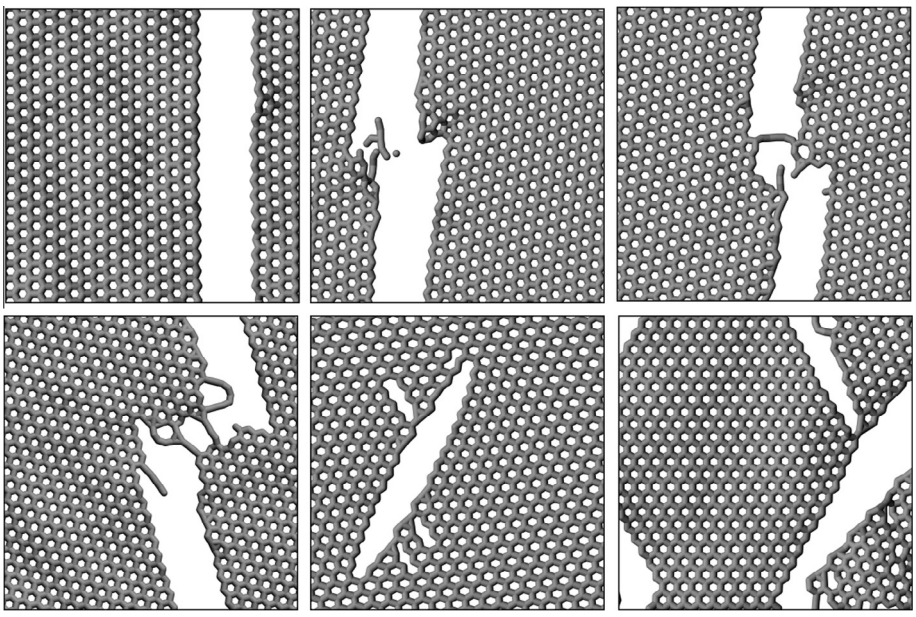

Fig. 4 – The graphene structures appearing at the fracture stage for the tensile directions of orientation angles of 0°, 6.6°, 8.2° (from left to right in the top panel), 16.1°, 23.4°, and 30° (from left to right in the bottom panel), respectively. Their equivalent chiral notations are (1,1), (3,2), (5,3), (3,1), (7,1) and (1,0), respectively.

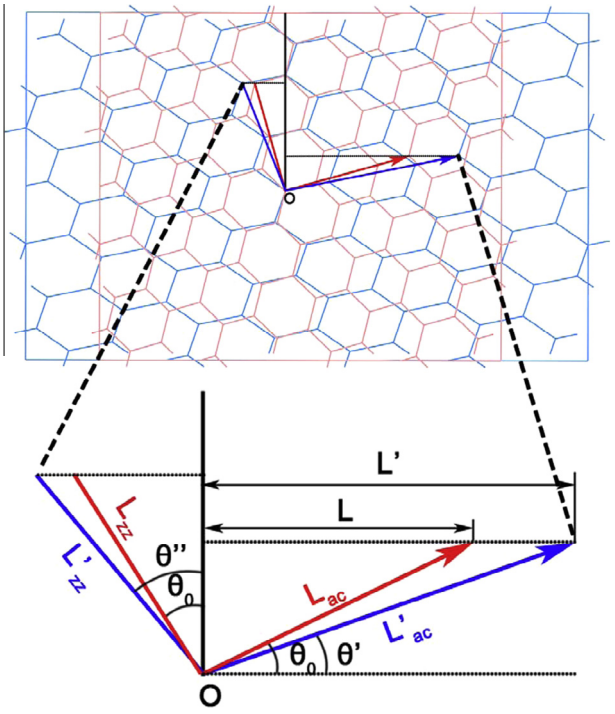

Fig. 5 – (a) The geometric variations of graphene occurring in the uniaxial tensile process. (b) The geometric diagram relating the angles of θ_0, θ', and θ'' with the lengths along the armchair, zigzag, and tensile directions of graphene. The red line and arrow indicate the lengths along the armchair and zigzag directions in the original graphene structure, respectively, while the blue line and arrow indicate the lengths in those directions in the elongated structure. (A color version of this figure can be viewed online.)

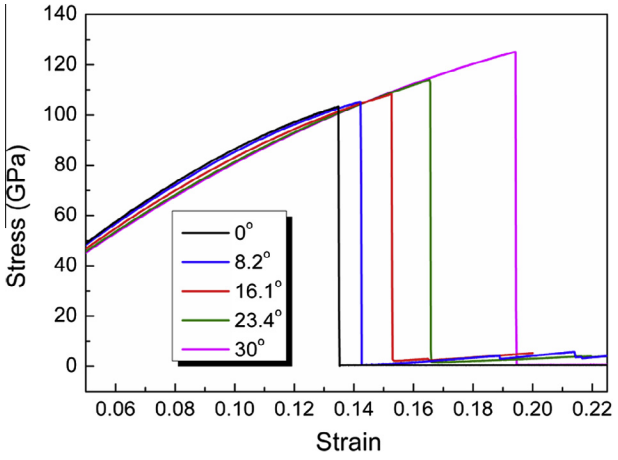

Fig. 6 – The tensile stress–strain curves of graphene obtained for a variety of tensile directions, the orientation angles of which are given in the box. (A color version of this figure can be viewed online.)

for the shape of the wells patterned in the SiO_2 substrates. We drilled elliptical wells (where the lengths of the short and long axes are 30 and 60 Å, respectively) instead of circular ones, in which the long-axis of the elliptical well was oriented in parallel with either the armchair or zigzag directions of the graphene to see any possible anisotropic effects (Fig. 7b). The diameter of the indenter is around 20 Å, and the force exerted on each atom due to the indenter is given by:

$$F(r) = K(r - R)^2 \quad (7)$$

where K is the specified force constant, r is the distance from each atom to the center of the indenter, and R is the radius of

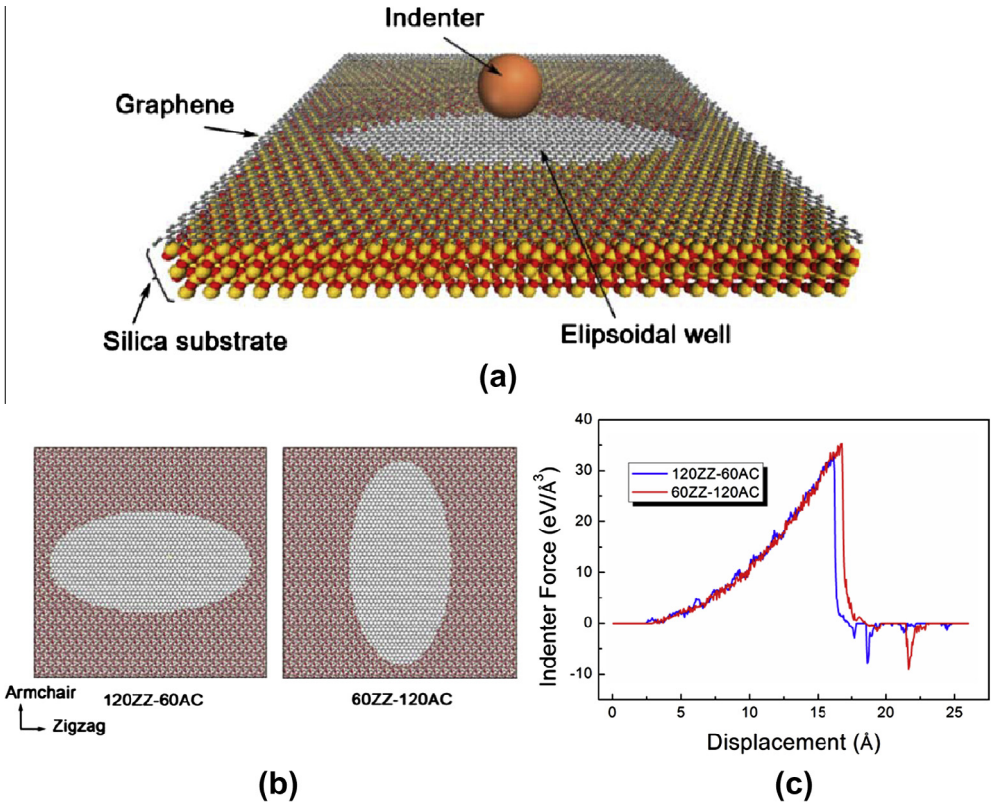

Fig. 7 – (a) The indentation simulation system employed in the study of the two-dimensional tensile system, where carbon, silicon, and oxygen atoms are shown in gray, yellow, and red, respectively. (b) Two differently oriented elliptical wells that are patterned in the silica substrate. (c) The measured values of the force exerted on an indenter as it gradually moves down for the indentation of graphene membrane. (A color version of this figure can be viewed online.)

the indenter. The force is repulsive and $F(r) = 0$ for $r > R$. Here, K and R are set to be 1000 eV/Å^3 and 10 Å, respectively. Meanwhile, details on the force field sets for graphene membrane, SiO_2 substrate, and the interaction between them are given in supplemenatry data.

As the indenter gradually moved downward, we measured the force exerted on the indenter for the above two systems where the elliptical wells of the substrates are differently oriented to each other. We obtained essentially the same result as that obtained in the uniaxial tensile process as follows. These indentation systems showed very similar elastic behaviors quantitatively and qualitatively, regardless of the well orientation (Fig. 7c). This means that our conclusion of the isotropic elastic behavior of graphene, established in its uniaxial (1D) tensile mechanics, is still operative for the 2D tensile systems. However, in contrast to their similar elastic behaviors, they yielded distinctly different values for the maximum indenter force (*i.e.*, the breaking force) and its corresponding indenter position (Fig. 7c). When the longer axis of the elliptical well is aligned in parallel with the armchair direction (denoted as 60ZZ-120AC), it requires a larger breaking force and greater movement of the indenter (34.71 ± 0.48 eV/Å and 16.60 ± 0.13 Å, respectively) compared to those required (32.72 ± 0.59 eV/Å and 16.09 ± 0.11 Å, respectively) in the other configuration (denoted as 120ZZ-60AC).

This anisotropic difference can be explained as follows. The effective tensile strain of graphene along the short axis direction (*i.e.*, the shortest radius direction) of an elliptical well should be greater than that in any of the other tensile directions, for the same amount of movement of the indenter. Furthermore, the fracture of graphene will be critically influenced by the deformation along the weakest tensile direction (namely, the armchair direction). In this context, 120ZZ-60AC should be weaker than 60ZZ-120AC with respect to the indentation because the short axis direction of an elliptical substrate well coincides with the armchair direction of the graphene membrane for 120ZZ-60AC. This conjecture is in good agreement with the above simulation result.

On the basis of a continuum model for a linear elastic, circular membrane under a spherical indenter, the tensile strength of graphene can be estimated from the measured value of the breaking force using the following equation [5,45]:

$$\sigma_{\mathrm{m}}^{2\mathrm{D}} = \left(\frac{FE^{2\mathrm{D}}}{4\pi R}\right)^{\frac{1}{2}} \tag{8}$$

where $\sigma_{\mathrm{m}}^{2\mathrm{D}}$ is the maximum tensile stress, and $E^{2\mathrm{D}}$ is a fitting parameter which is set to 342 N m^{-1} as suggested by Lee et al. [5], R is the tip radius, and F is the breaking force.

Based on this relationship, the tensile strengths of 60ZZ-120AC and 120ZZ-60AC were evaluated to be 116.15 and 112.78 GPa, respectively. They are within reasonable range considering the tensile strengths obtained from the uniaxial tensile simulations. Though this fracture behavior is qualitatively consistent with our understanding for the uniaxial

tensile fracture of graphene, the anisotropic response observed in the indentation process is much weakened compared to the uniaxial tensile process. We attribute this attenuation effect to the following two factors.

First, to the degree that a certain tensile direction (indentation tensile deformation is composed of many individual tensile deformations along the various tensile directions) approaches the short axis direction of an elliptical well, both the in situ strain (a current value) and fracture strain (a threshold value) pertaining to that tensile direction become larger for 60ZZ-120AC, whereas the in situ and fracture strains increases and decreases, respectively, for 120ZZ-60AC. Owing to such a cancelation effect, a critical tensile direction, which determines the fracture point, does not coincide with the short axis direction (zigzag direction) of an elliptical well for 60ZZ-120AC. Instead, a critical tensile direction should be located between the short axis (zigzag) direction and the armchair direction that intersects the short axis direction with an angle of 30° (it should be noted that this direction is not the long axis armchair direction of an elliptical well), lowering the magnitude of the breaking force in comparison with that of a fracture occurring along the short axis (zigzag) direction (see Fig. 8). This decrement will eventually weaken the anisotropic effect on the fracture strength. Regarding this point, increasing the aspect ratio of an elliptical well will help obtain a more distinct anisotropic fracture behavior of graphene indentation.

This conjecture shown in Fig. 8 is indeed verified by simulating the fractured structures of graphene membranes under nanoindentation, in which the fracture line is created along the longest axis direction (*i.e.*, the zigzag lines that are perpendicular to the shortest axis direction) for 120ZZ-60AC while it emerges along the zigzag lines in the direction which intersects the shortest axis direction with an angle of 60° for 60ZZ-120AC (Fig. 9 and Supplementary Movies 2–5).

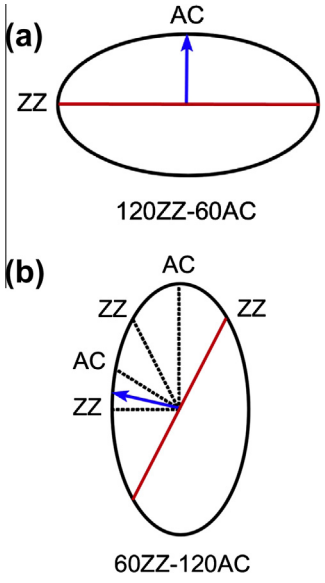

Fig. 8 – The underlying fracture mechanism in the indentation of (a) 120ZZ-60AC and (b) 60ZZ-120AC. The blue arrow denotes a critical tensile direction that determines the fracture point of the indentation process while the red lines denote a fracture line which agrees well with the simulation result shown in Fig. 9. (A color version of this figure can be viewed online.)

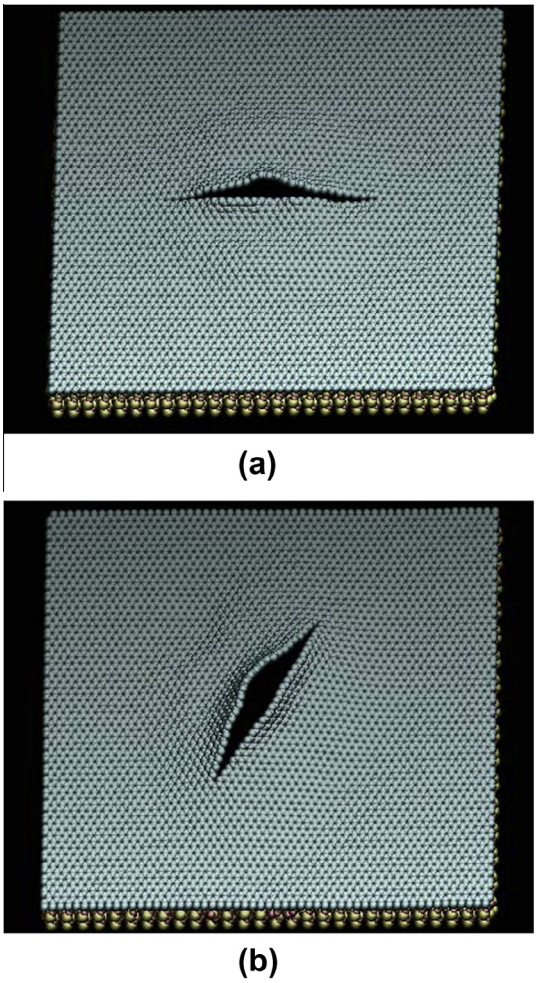

Fig. 9 – The fractured structures of graphene membranes under nanoindentation for (a) 120ZZ-60AC and (b) 60ZZ-120AC. The orientations of the graphene membranes and substrate elliptical wells are the same as those in Fig. 7b. (A color version of this figure can be viewed online.)

Second, the size allowed for the intersection angle between the critical tensile direction of the graphene membrane and the short axis direction of an elliptical well is at most as small as 30° (accordingly, the difference between the two radii of an elliptical well corresponding to these directions would be also small) and thus, the indentation process always brings severe impact on the fracture of the graphene membrane regardless of the orientation of the elliptical well patterned in the substrate. This is an inevitable factor arising from the inherent structure of graphene, which can hardly be resolved to promote the fracture anisotropicity in the indentation of graphene.

It is noteworthy that the indentation scheme employed in this study, which utilizes elliptical substrate wells, can be directly used in experiments for the anisotropic mechanical study of graphene, since an indentation scheme using circular substrate wells is already well established experi-

mentally [5]. This experimental application will have great importance because the anisotropic tensile fracture behavior of graphene has never been experimentally validated. In fact, we have examined both effects of using an anisotropic shape of the indenter tip and an anisotropic shape of the substrate well for this study and we found that the latter method is much more efficient than the former method. We were not able to observe the anisotropic mechanical response of graphene using the tip-variation method.

4. Conclusion

By exploring the entire range of tensile orientations for the first time, we revealed the unique orientation-dependent fracture behavior of graphene using molecular dynamics simulations. After defining an orientation angle as the angle made between a certain tensile direction and the armchair direction of graphene, we performed a series of uniaxial tensile simulations by gradually increasing the orientation angle from 0° (armchair direction) to 30° (zigzag direction), which covers the entire range of tensile orientations due to the sixfold symmetry of graphene. Noticeably, our calculations indicate that both the tensile strength and strain remain almost constant up to an orientation angle of ~12°, and then rapidly increase as the orientation angle increases. This increase pattern resembles an exponential growth curve in contrast to the inverse-sinusoidal growth curve of the brittle fracture response, resulting in a remarkable degradation of the tensile strength in comparison with the brittle fracture case. We suggested a model to explain its physical origin considering its exceptional, highly stretched structure, which reproduced the simulation results well. In contrast to its anisotropic fracture response, graphene exhibits quasi-isotropic elastic behavior for all tensile orientations. We found that such anisotropic/isotropic features of fracture/elasticity are also applicable to 2D tensile systems (indentation) but the fracture anisotropicity is much attenuated due to the inherent sixfold-symmetric structure of graphene. Based on the simulation results, we finally presented a numerical platform that can precisely predict the fracture behavior of graphene for a complete range of tensile orientations under a wide range of operating temperatures.

Acknowledgement

This work was supported by the "Nano-Material Technology Development Program through the National Research Foundation of Korea (NRF)" funded by the Ministry of Education, Science and Technology (2012035324) and "Futuristic Fundamental Research Program" funded by Korea Institute of Science and Technology.

Appendix A. Supplementary data

Supplementary data associated with this article can be found, in the online version, at http://dx.doi.org/10.1016/j.carbon.2013.09.051.

REFERENCES

[1] Bolotin KI, Sikes KJ, Jiang Z, Klima M, Fudenberg G, Hone J, et al. Ultrahigh electron mobility in suspended graphene. Solid State Commun 2008;146:351–5.
[2] Chen JH, Jang C, Xiao S, Ishigami M, Fuhrer MS. Intrinsic and extrinsic performance limits of graphene devices on SiO_2. Nat Nanotechnol 2008;3:206–9.
[3] Seol JH, Jo I, Moore AL, Lindsay L, Aitken ZH, Pettes MT, et al. Two-dimensional phonon transport in supported graphene. Science 2010;328:213–6.
[4] Balandin AA, Ghosh S, Bao W, Calizo I, Teweldebrhan D, Miao F, et al. Superior thermal conductivity of single-layer graphene. Nano Lett 2008;8(3):902–7.
[5] Lee C, Wei X, Kysar JW, Hone J. Measurement of the elastic properties and intrinsic strength of monolayer graphene. Science 2008;321:385–8.
[6] Liu F, Ming PM, Li J. Ab initio calculation of ideal strength and phonon instability of graphene under tension. Phys Rev B 2007;76:064120.
[7] Vadukumpully S, Paul J, Mahanta N, Valiyaveettil S. Flexible conductive graphene/poly(vinyl chloride) composite thin films with high mechanical strength and thermal stability. Carbon 2011;49:198–205.
[8] Fang M, Wang K, Lu H, Yang Y, Nutt S. Covalent polymer functionalization of graphene nanosheets and mechanical properties of composites. J Mater Chem 2009;19:7098–105.
[9] Zandiatashbar A, Picu CR, Koratkar N. Control of epoxy creep using graphene. Small 2012;8(11):1676–82.
[10] Potts JR, Dreyer DR, Bielawski CW, Ruoff RS. Graphene-based polymer nanocomposites. Polymer 2011;52:5–25.
[11] Layek RK, Samanta S, Chatterjee DP, Nandi AK. Physical and mechanical properties of poly(methyl methacrylate)-functionalized graphene/poly(vinylidine fluoride) nanocomposites: piezoelectric b polymorph formation. Polymer 2010;51:5846–56.
[12] Goncalves G, Marques PA, Barros-Timmons A, Bdkin I, Singh MK, Emami NE, et al. Graphene oxide modified with PMMA via ATRP as a reinforcement filler. J Mater Chem 2010;20:9927–34.
[13] Fang M, Wang KG, Lu HB, Yang YL, Nutt S. Single-layer graphene nanosheets with controlled grafting of polymer chains. J Mater Chem 2010;20:1982–92.
[14] Sahoo NS, Pan Y, Li L, Chan SH. Graphene-based materials for energy conversion. Adv Mater 2012;24:4203–10.
[15] Dai L. Functionalization of graphene for efficient energy conversion and storage. Acc Chem Res 2013;46(1):31–42.
[16] Kamat PV. Graphene-based nanoassemblies for energy conversion. J Phys Chem Lett 2011;2(3):242–51.
[17] Yuk JM, Park JW, Ercius P, Kim KP, Hellebusch DJ, Crommie MF, et al. High-resolution EM of colloidal nanocrystal growth using graphene liquid cells. Science 2012;336(6):61–4.
[18] Griffith AA. The phenomena of rupture and flow in solids. Philos Trans R Soc Lond A 1921;221:163–98.
[19] Lawn B. Fracture of brittle solids. 2nd ed. London: Cambridge University Press; 1993.
[20] Thomason PF. Ductile fracture of metals. 1st ed. Oxford: Pergamon; 1990.
[21] Callister WD. Fundamentals of materials science and engineering. 2nd ed. New York: John Wiley and Sons; 2004.
[22] Zhao H, Min K, Aluru NR. Size and chirality dependent elastic properties of graphene nanoribbons under uniaxial tension. Nano Lett 2009;9(8):3012–5.
[23] Wang MC, Yan C, Ma L, Hub N, Chen MW. Effect of defects on fracture strength of graphene sheets. Comput Mater Sci 2009;54:236–9.

[24] Jhon YI, Zhu SE, Ahn JH, Jhon MS. The mechanical responses of tilted and non-tilted grain boundaries in graphene. Carbon 2012;50:3708–16.
[25] Grantab R, Shenoy VB, Ruoff RS. Anomalous strength characteristics of tilt grain boundaries in graphene. Science 2010;330:946–8.
[26] Stone AJ, Wales DJ. Theoretical studies of icosahedral C60 and some related species. Chem Phys Lett 1986;128(5–6):501–3.
[27] Thrower PA. The study of defects in graphite by transmission electron microscopy. Chem Phys Carbon 1969;5:217–320.
[28] Malola S, Hakkinen H, Koskinen P. Structural, chemical, and dynamical trends in graphene grain boundaries. Phys Rev B 2010;81:165447.
[29] Khare R, Mielke S, Paci J, Zhang S, Ballarini R, Schatz G, et al. Coupled quantum mechanical/molecular mechanical modeling of the fracture of defective carbon nanotubes and graphene sheets. Phys Rev B 2007;75:075412.
[30] Cadelano E, Palla PL, Giordano S, Colombo L. Nonlinear elasticity of monolayer graphene. Phys Rev Lett 2009;102:235502.
[31] Wei X, Fragneaud B, Marianetti CA, Kysar JW. Nonlinear elastic behavior of graphene: ab initio calculations to continuum description. Phys Rev B 2009;80:205407.
[32] Pereira VM, Castro-Neto AH. Tight-binding approach to uniaxial strain in graphene. Phys Rev B 2009;80:045401.
[33] Hernandex E, Goze C, Bernier P, Rubio A. Elastic properties of C and $B_xC_yN_z$ composite nanotubes. Phys Rev Lett 1998;80(20):4502–5.
[34] Pei QX, Zhang YW, Shenoy VB. A molecular dynamics study of the mechanical properties of hydrogen functionalized graphene. Carbon 2010;48:898–904.
[35] Zhao H, Aluru NR. Temperature and strain-rate dependent fracture strength of graphene. J Appl Phys 2010;108:064321.
[36] Chien SK, Yang YT, Chen CK. A molecular dynamics study of the mechanical properties of graphene nanoribbon-embedded gold composites. Nanoscale 2011;3:4307–13.
[37] Plimpton S. Fast parallel algorithms for short-range molecular dynamics. J Comput Phys 1995;117:1–19.
[38] Stuart SJ, Tutein AB, Harrison JA. A reactive potential for hydrocarbons with intermolecular interactions. J Chem Phys 2000;112(14):6472–86.
[39] Xu Z, Buehler MJ. Nanoengineering heat transfer performance at carbon nanotube interfaces. ACS Nano 2009;3(9):2767–75.
[40] Los JH, Pineau N, Chevrot G, Vignoles G, Leyssale JM. Formation of multiwall fullerenes from nanodiamonds studied by atomistic simulations. Phys Rev B 2009;80:155420.
[41] Qi Z, Zhao F, Zhou X, Sun Z, Park HS, Wu H. A molecular simulation analysis of producing monatomic carbon chains by stretching ultranarrow graphene nanoribbons. Nanotechnology 2010;21:265702.
[42] Tuckerman ME, Mundy CJ, Balasubramanian S, Klein ML. Modified nonequilibrium molecular dynamics for fluid flows with energy conservation. J Chem Phys 1997;106(13):5615–21.
[43] Dumitrica T, Hua M, Yakobson BI. Symmetry-, time-, and temperature-dependent strength of carbon nanotubes. Proc Natl Acad Sci USA 2006;103(16):6105–9.
[44] Bucciarelli LL. Engineering mechanics for structures. New York: Dover Publications; 2009.
[45] Bhatia NM, Nachbar W. Finite indentation of an elastic membrane by a spherical indenter. Int J Nonlinear Mech 1968;3:307–24.